In: 2024 International Conference on Unmanned Aircraft Systems (ICUAS), 4-7 June 2024, Chania - Crete, Greece. DOI:10.1109/ICUAS60882.2024.10557007

authors' accepted manuscript

A Modular UAV Hardware Platform for Aerial Indoor Navigation Research and Development

Kyriakos M. Deliparaschos, Savvas G. Loizou, and Argyrios C. Zolotas

***Abstract*— This study introduces a specialised hardware platform designed for indoor navigation, featuring a quadrotor equipped with either a NVIDIA Jetson Nano or a Z-turn Zynq onboard computer. The onboard computer communicates via ROS2 with the flight controller, the Inertial Measurement Unit (IMU), Ultra-WideBand (UWB) localisation system, stereo camera, Light Detection and Ranging (LiDAR), and ultrasonic sensors. The focus is on creating a low-cost modular Unmanned Aerial Vehicle (UAV) system adaptable to various indoor navigation applications. The modular design encompasses different onboard computer platforms and sensor configurations, allowing for easy adaptation to research experiment setups. The objective is to facilitate the transition from simulated and simplified laboratory experiments to deploying aerial robots in challenging real-world conditions. The paper explores the hardware architecture and Robot Operating System 2 (ROS2)-based communication system of the UAV and provides a weight analysis and power estimation.**

I. INTRODUCTION

Unmanned aerial vehicles (UAVs) have undoubtedly opened new frontiers in research, particularly in aerial navigation [1], [2]. While there is extensive research efforts directed towards deploying UAV systems with various navigation approaches (and in particular for the challenging aspect of aerial indoor navigation), a substantial portion of the proposed methodologies rely mostly on simulations [3]. Unfortunately, these approaches often fall short of meeting real-world deployment requirements. This paper introduces a low-cost modular UAV hardware platform developed to, particularly, enable aerial indoor navigation research development and system validation. By focusing on modularity, the platform provides a flexible and adaptable baseline for experiments, enabling researchers to customise and scale, within reasonable payload requirements, their setups according to the specific requirements of indoor environments. This approach not only accelerates the rate of development but also enables investigation of the precision and reliability of UAV navigation within indoor spaces. Through a comprehensive exploration of its architecture, capabilities, and potential applications, we aim to highlight how this platform can facilitate the advancement of UAV indoor navigation research [4][5].

K. M. Deliparaschos is with the Electrical and Computer Engineering and Informatics Department, Cyprus University of Technology, Limassol, Cyprus k.deliparaschos@cut.ac.cy.

S. G. Loizou is with the Department of Mechanical Engineering and Materials Science and Engineering, Cyprus University of Technology, Limassol, Cyprus savvas.loizou@cut.ac.cy.

A. C. Zolotas is with the Centre for Autonomous and Cyber-Physical Systems, SATM, Cranfield University, Cranfield, UK a.zolotas@cranfield.ac.uk.

II. HARDWARE DESCRIPTION

The finalised quadrotor project comprises diverse individual components used to complete the project. This section provides an overview of the key components chosen, accompanied by a concise analysis of the decision-making process.

A. IMU

An Inertial Measurement Unit (IMU) is a device that utilises a combination of accelerometer, gyroscope, and magnetometer sensors to ascertain a body's orientation, velocity, and gravitational forces. It is commonly employed alongside other sensors, such as those based on vision or wireless technology, to improve the accuracy of pose estimation. In instances where other sensors are unavailable, the IMU may function as the primary sensor. The IMU delivers measurements of a quadrotor's orientation through the three Euler angles: roll, pitch, and yaw. The Pixhawk PX4 Flight Control Unit (FCU) incorporates three internal sensor chips, primarily the Invensense MPU 6000 as the main 3-axis accelerometer/gyroscope, ST Micro L3GD20 3-axis 16-bit gyroscope, and ST Micro LSM303D 3-axis 14-bit accelerometer/magnetometer.

B. FCU

The responsibility of controlling the drone's movement and adjusting the power delivered to each motor is assigned to the Flight Controller Unit (FCU). Flight controllers are capable of measuring the drone's level and speed, utilising this information to correct its orientation during flight. In this project, the chosen flight controller is the Readytosky Pixhawk PX4 2.4.8 32-bit. This selection was made based on the controller's additional features beyond the standard gyroscope and accelerometer sensors found in all flight controllers. The Pixhawk incorporates a barometer, magnetometer, and IMU, enhancing the accuracy and consistency of flight performance. Furthermore, the Pixhawk is a 32-bit controller with I2C and SPI interfaces and has the flexibility to run either the PX4 or ArduPilot flight stack.

C. Onboard Computer

The quadrotor's onboard computer, operated through the Robot Operating System 2 (ROS2), manages essential quadrotor functions, including image recognition from stereo camera frames, processing ground Ultra Wide Band (UWB) sensor data, analysing point clouds from the LiDAR sensor, integrating sensor measurements from the flight controller, transmitting commands to the flight controller, and relaying

Published by IEEE. This is the Author Accepted Manuscript issued with: Creative Commons Attribution License (CC:BY 4.0).
The final published version (version of record) is available online at DOI:10.1109/ICUAS60882.2024.10557007. Please refer to any applicable publisher terms of use.

video to the ground station. When selecting a suitable computer for our system, we sought a powerful yet lightweight and energy-efficient option. Our primary choice was the NVIDIA Jetson Nano Development Kit, featuring a 4-core 1.43GHz processor with 4GB of memory and a 128-core Maxwell GPU [6]. Weighing 142 grams and using up to 15W at maximum power, its NVIDIA CUDA core GPU offers broader compatibility for software running object detection algorithms. This CPU-GPU combination ensures ample computational power for running object detection and other concurrently executed software. Additionally, the Jetson Nano enables experimentation with NVIDIA-specific libraries for deep learning and computer vision, making it the preferred choice for our quadrotor application.

Moreover, we integrated the MYIR Z-turn FPGA board [7] with an AMD (formerly Xilinx) Zynq-7020 SoC for real-time point cloud processing. The Z-turn board, at least twice as power-efficient compared to the Jetson Nano, enhances the processing capabilities for point cloud data, providing an efficient solution for our quadrotor system. Utilising a dedicated Delaunay triangulation core [8], developed by the authors in prior work, on the FPGA portion (PL) of the Zynq SoC further enhances its ability to process point cloud data efficiently. Moreover, the Z-turn FPGA board features an on-board three-axis acceleration sensor and temperature sensor, further augmenting its capabilities for various applications in our quadrotor system.

D. Camera

Exploring various camera options for our system, one possibility involved using a single, basic RGB camera to capture video data for an object detection algorithm, facilitating the identification of object locations. However, we acknowledged that this setup might pose challenges in accurately determining the distance to most objects. To address this limitation, we opted for a ZED 2 stereo camera [9], utilising the relative pixel differences between the two images to compute distances on the computer. The stereo camera connects via USB to the Jetson Nano. A drawback of this approach is the substantial processing power required, particularly when running a computationally intensive object detection algorithm on the same system.

Additionally, we considered a less computationally demanding approach by employing a LiDAR sensor instead of two RGB cameras. Utilising the point cloud generated by the LiDAR sensor, we can employ the reconstructed surface for object recognition while simultaneously determining the distance to the objects.

E. LiDAR

The light detection and ranging (LiDAR) sensor aids in detecting obstacles within the environment [10]. We've integrated a Hokuyo URG-04LX-UG01 2D LiDAR [11][12] onto the UAV. This specific LiDAR offers a range from 20mm to 5500m (with a 1mm resolution), covering a 240°scan window with an angular resolution of 0.36°. It features low power consumption (2.5W) and a lightweight design (138g).

F. Ultrasonic Sensors

We selected a microcontroller, specifically the Atmel ATMEGA328P on an Arduino Pro Mini board, to oversee four laterally mounted HC-SR04 ultrasonic range sensors. Directly invoking the ultrasonic sensor from the Jetson Nano could result in suboptimal performance due to the Nano's real-time processing limitations, potentially leading to inaccurate distance measurements. A more effective approach involves incorporating a compact microcontroller, such as the Arduino Pro Mini, which, through I2C communication, can conduct distance measurements and relay results back to the Jetson Nano, thereby enhancing the reliability of distance calculations.

The chosen architecture, based on the Atmel ATMEGA328P microcontroller on an Arduino Pro Mini board, boasts an 8-bit 16 MHz design. This IC is well-suited for driving ultrasonic range sensors and transmitting distance information to the processing module via UART. The choice is attributed to its compact form factor, low weight, minimal power consumption, extensive documentation, and user-friendly nature through the Arduino development platform.

G. WiFi Communication

To facilitate communication between the drone computer and a ground control computer for sending video data, WiFi capability is essential. As the Jetson Nano lacks a built-in WiFi module, we opted for the AC1300 Archer T3U Mini Wireless MU-MIMO USB Adapter. Choosing a USB WiFi module over a WiFi card was intentional, as the latter would have necessitated the installation of a separate antenna for proper operation. The USB module, equipped with a small antenna, offered a more straightforward integration with the overall system.

The AC1300 Archer T3U USB module was specifically selected for its compatibility with USB 3.0, available on the Jetson Nano, allowing for data speeds of up to 4,800 Mbps—ten times faster than USB 2.0 ports. It delivers WiFi speeds of 400 Mbps on the 2.4GHz band and 867 Mbps on the 5GHz band. The AC1300, combining 802.11ac WiFi with USB 3.0, proves ideal for HD streaming and large file downloads. Additionally, the AC1300 features MU-MIMO technology, enabling two simultaneous data streams, thereby enhancing the throughput and efficiency of the entire network when paired with a compatible MU-MIMO router.

H. UWB Sensors

Ultra-Wideband (UWB) is a wireless communication technology that utilises short pulses with low energy over a wide bandwidth, making it highly resistant to multipath interference. Unlike conventional radio frequency identification (RFID) systems operating on single bands, UWB transmits over a broad spectrum of radio frequencies, decreasing the power spectral density. This characteristic allows UWB-based systems to avoid interference with other RF signals.

UWB's unique features include the ability to precisely measure Time-of-Flight (ToF), facilitating accurate distance estimation. This makes UWB a popular choice for localisation in indoor environments. Localisation using UWB involves placing wireless transmitters, known as anchors, at specific locations and using a UWB receiver, called a tag, on the quadrotor to log the arrival times of UWB signals and calculate the quadrotor's position in space[1].

The selected UWB system is based on the Pozyx system [13], utilising the Decawave DWM1000 chip.

I. Battery

The drone will be powered by a Lithium Polymer (LiPo) battery, connected to the power distribution board (PDB) to distribute power to the various components. The selected battery is a 3S1P LiPo Battery (i.e. 3 cells connected in series) with specifications of 11.1 volts, 4400 mAh, 30C discharge rate, and a weight of 340g. The choice of this battery was primarily determined by two key specifications: its total output voltage and weight.

J. DC-to-DC Converter

To supply power to the Jetson Nano through the drone's power distribution board, we employed a buck converter[2]. The Jetson Nano is designed to receive a DC power supply of 5V with a maximum current of 4 Amps, ensuring a sufficient power supply, especially during computationally demanding processes such as running an object detection algorithm, preventing a CPU shutdown.

K. Motors

We selected four A2212 brushless DC motors (BLDC) rated at 1000kV (1000RPM/V)[3] with 80% maximum efficiency. Each motor is powered by a 30A electric speed controller (ESC) and paired with 1045 (pitch 10 in, diameter 4.5 in) propellers (CW, CCW), producing 800g of thrust.

On a side note, brushless DC motors defy their name; they're not DC motors but rather AC polyphase synchronous motors. Through electronics, DC is converted to AC, generating a multiphase rotating magnetic field. In contrast, brushed DC motors utilise brush contacts as electro-mechanical DC to AC converters, while brushless DC motors employ electronics to drive the coils with switched DC current, effectively producing AC.

L. RC Receiver

The Radiolink R8EF used in this UAV implementation is an 8-channel receiver operating at a 2.4 GHz frequency, connected to the quadcopter's FCU. More precisely, the SBUS/Channel 1 is linked to the Pixhawk RC input. This receiver's function is to transmit signals to the controller based on stick movements from the radio control transmitter, enabling control over the quadcopter's motion as required.

[1]The locations of the anchors can also be inferred if they are in a certain formation and the initial position of the tag is known.

[2]A buck converter, also known as a step-down converter, is a DC-to-DC converter that reduces voltage while simultaneously increasing current from its input (supply) to its output (load). This converter falls within the category of switched-mode power supplies.

[3]A 3-cell LiPo battery, with a nominal voltage of 11.1V, would theoretically cause a 1000kV motor to spin at 11,100 RPM without any load.

III. SYSTEM DESCRIPTION

A. Hardware Architecture

The drone system architecture comprises several key components seamlessly integrated to ensure efficient and autonomous operation as shown in Fig.1. At its core is the Jetson Nano, serving as the central processing unit responsible for high-level computations and decision-making. Connected to the Jetson Nano is a flight controller, in this case, the Readytosky Pixhawk, which manages the drone's movement and motor control. Alternatively, the authors have examined the use of the Z-turn FPGA board with a Zynq SoC as an alternative to the Jetson Nano, exploring different possibilities for the system's central processing unit.

Sensory input is facilitated by various sensors, including a stereo camera for image recognition, an Inertial Measurement Unit (IMU) for orientation data, Ultra-WideBand (UWB) sensors for localisation, and a LiDAR sensor for point cloud data. These sensors collectively provide essential information for navigation and obstacle avoidance.

To power the system, a Lithium Polymer (LiPo) battery is utilised, connected to a power distribution board (PDB) that distributes power to all components. Additionally, a DC-to-DC converter ensures the Jetson Nano receives the appropriate voltage from the drone's power supply.

For communication, a WiFi module, specifically the AC1300 Archer T3U Mini Wireless MU-MIMO USB Adapter, enables data exchange with a ground control station. The overall architecture is designed for modularity, allowing flexibility in adjusting configurations for different scenarios and experiments.

B. Coordinate Systems

To determine the location of the quadrotor in space and the relative locations of surrounding objects around it, we define two coordinate frames using the standard right-handed robotics convention as shown in Fig.2. The Earth's inertial frame $\{E\}$ follows the East-North-Up (ENU) reference system where $+x$ axis points to the east, $+y$ to the north and $+z$ points upwards based on the right-hand rule. The Body frame of the quadrotor $\{B\}$ is coincident to the origin and thus to the absolute position of the quadrotor, *i.e.* $[x,\ y,\ z]$, while it follows the Forward-Left-Up (FLU) which gives forward horizontal, left horizontal and up vertical movement along its $+x$, $+y$ and $+z$ axis, respectively.

C. Quadrotor Aircraft Dynamical Model

The quadrotor is a naturally unstable non-linear complex system composed of four rotors, as the name suggests. Each rotor is made up of a propeller and a motor that generates an angular velocity ω_i, resulting in a thrust force f_i, where i refers to the number of the motor as depicted in Fig.2. Two rotors rotate clockwise while the other two rotate counterclockwise to prevent unwanted rotation of the quadrotor

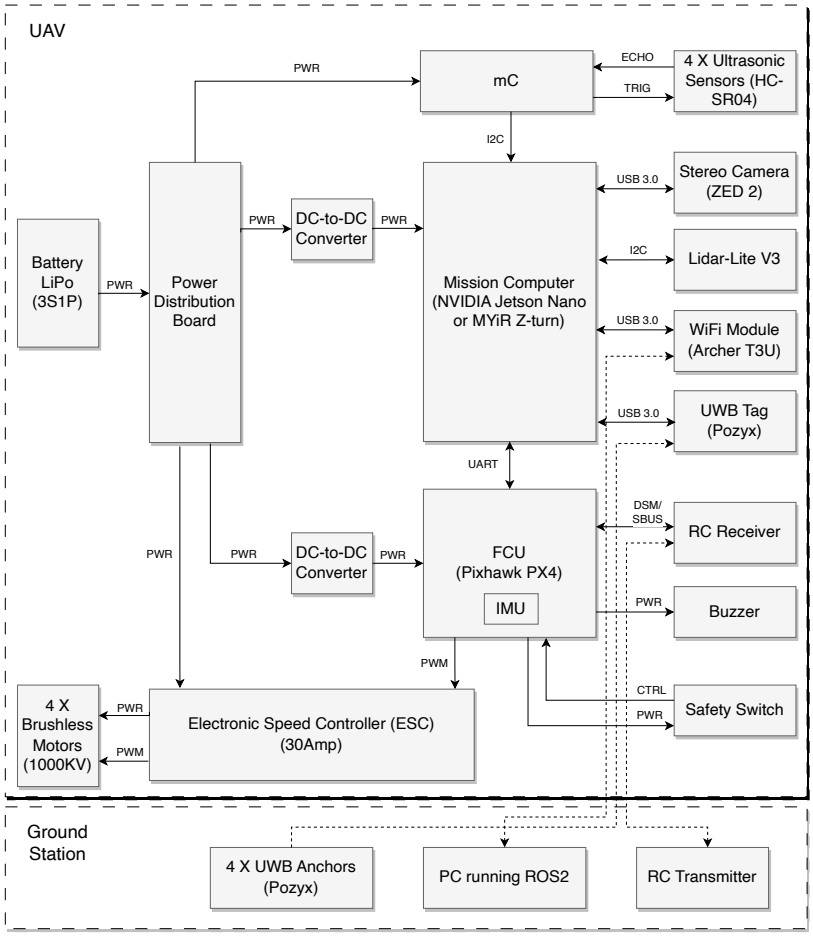

Fig. 1. Quadrotor system architecture.

body in the yaw (ψ) direction (conservation of angular momentum). The angular velocities of the rotors correspond to specific rotational coordinates, $\boldsymbol{\eta} = (\phi, \theta, \psi) \in \mathbb{R}^3$, and move the quadrotor to different translational coordinates, $\boldsymbol{\xi} = (x, y, z) \in \mathbb{R}^3$, in the Earth inertial frame E. The orientation of the quadrotor is defined by the Euler angles ϕ, θ and ψ. ϕ (roll) is the angle around the x-axis, θ (pitch) is the angle around the y-axis, and ψ (yaw) is the angle around the z-axis. The translational coordinates x, y and z represent the centre of mass of the quadrotor relative to the Earth inertial frame. The translational and rotational equations of motion for a quadrotor in Earth frame are described using the Newton-Euler formalism [14], [15] and [16], respectively. These equations take into account relatively small quadrotor movement angles

$$\ddot{x} = \frac{f_T}{m}\left(c\phi s\theta c\psi + s\psi s\phi\right), \quad \ddot{\phi} = \frac{I_y - I_z}{I_x}\dot{\theta}\dot{\psi} + \frac{\tau_x}{I_x},$$
$$\ddot{y} = \frac{f_T}{m}\left(c\phi s\theta s\psi - c\psi s\phi\right), \quad \ddot{\theta} = \frac{I_z - I_x}{I_y}\dot{\phi}\dot{\psi} + \frac{\tau_y}{I_y},$$
$$\ddot{z} = \frac{f_T}{m}\left(c\phi c\theta\right) - g, \quad \ddot{\psi} = \frac{I_x - I_y}{I_z}\dot{\phi}\dot{\theta} + \frac{\tau_z}{I_z},$$

where m represents the mass of the quadrotor, f_T represents the total thrust force, and g represents the acceleration due to gravity. The terms τ_θ, τ_ϕ, and τ_ψ are the pitch torque, roll torque, and yaw torque, respectively and they depend on the angular velocities of the rotors Ω_i [17]. Furthermore, I_x, I_y, and I_z are the moments of inertia of the quadrotor's symmetric rigid body around its three axes.

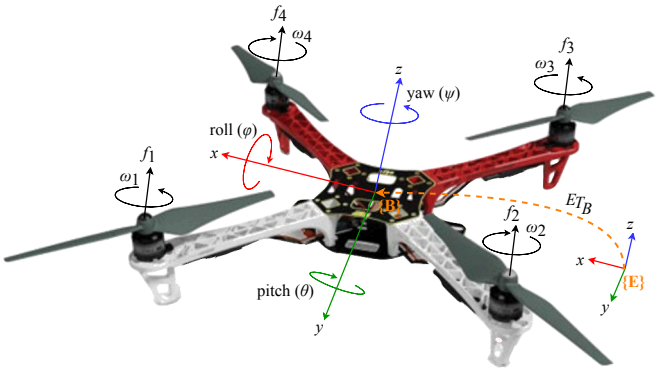

Fig. 2. F450 quadrotor model with coordinate frame.

A simplified linearised model can be obtained around the hovering equilibrium point by small-angle approximation (*i.e.* assuming that the rotational angles of the system

are relatively small), which implies that $\dot{\phi}, \dot{\theta}, \dot{\psi} \simeq 0$, and $s\phi \simeq \phi, s\theta \simeq \theta, s\psi \simeq \psi$, with $c\phi = 1$, $c\theta = 1$, and $c\psi = 1$. The system state vector is defined as $\boldsymbol{x} = [x\ y\ z\ \phi\ \theta\ \psi\ \dot{x}\ \dot{y}\ \dot{z}\ \dot{\phi}\ \dot{\theta}\ \dot{\psi}]^T$. The hovering equilibrium point, $\bar{\boldsymbol{x}} = [\bar{x}\ \bar{y}\ \bar{z}\ 0\ 0\ 0\ 0\ 0\ 0\ 0\ 0\ 0]^T$, is reached when the total thrust is a constant control input of $f_T = mg$, reflecting the force necessary to hover the quadrotor at an arbitrary position $(\bar{x}, \bar{y}, \bar{z})$. The resulting linearised system is described by

$$\begin{aligned} \ddot{x} &= g\theta, \quad \ddot{y} = -g\phi, \quad \ddot{z} = \frac{f_T}{m}, \\ \ddot{\phi} &= \frac{\tau_x}{I_x}, \quad \ddot{\theta} = \frac{\tau_y}{I_y}, \quad \ddot{\psi} = \frac{\tau_z}{I_z}. \end{aligned} \tag{2}$$

D. Camera-Based Localisation

Camera-based detection of landmarks is a well-established approach for robot localisation. The method involves utilising a camera mounted on the quadrotor and a set of landmarks whose positions are known with respect to the global reference frame. Analysing the objects detected by the camera facilitates the estimation of the quadrotor's position. Given that a monocular camera is used, depth information about the landmarks can be obtained by analysing successive frames. This process enables the estimation of the relative position between a landmark and the camera. Once the relative position of the camera is known, the relative position of the quadrotor on which the camera is attached to, can be obtained and expressed in the global reference frame.

E. ROS2 Based Communication Architecture

The Robot Operating System (ROS), an open-source middleware, has found extensive application in robotics. Despite its strengths, ROS isn't well-suited for real-time embedded systems due to its inability to meet real-time requirements and its limited compatibility with operating systems. To overcome this challenge, ROS1 has undergone a substantial overhaul, resulting in ROS2, which leverages the Data Distribution Service (DDS). DDS is better suited for real-time distributed embedded systems because of its diverse transport configurations, such as deadline management and fault tolerance, as well as its scalability.

By using ROS2, a primary program can be subdivided into multiple subprocesses that operate concurrently and interact with each other. In ROS2, nodes represent processes, each assigned with a distinct task aimed at enhancing the overall system efficiency. Communication among these nodes occurs through a series of topics and services. Topics act as bridges facilitating the transfer of information, known as messages, from one node to another. Nodes publish and/or subscribe to topics to respectively send and/or receive these messages. Services operate on the request/response model; hence, one node offers a service that another node invokes using the service name. The node creating the service is the server, while the nodes calling the service are the clients. Topics are suitable for managing continuous data streams, while services are best utilised for blocking calls, making them ideal for remote procedure calls that terminate quickly.

The uXRCE-DDS middleware is employed within the PX4 to enable the publication and subscription of uORB messages on the Jetson Nano, mimicking ROS2 topics. This facilitates a swift and dependable integration between PX4 and ROS2, simplifying the process for ROS2 applications to access UAV information and issue commands. PX4 utilises an XRCE-DDS implementation that takes advantage of eProsima Micro XRCE-DDS [18]. The uXRCE-DDS middleware comprises a client operating on PX4 and an agent functioning on the Jetson Nano. These components facilitate bidirectional data exchange between them through a serial or UDP connection. Acting as a proxy for the client, the agent allows it to both publish and subscribe to topics within the global DDS data space. For PX4 uORB topics to be accessible on the DDS network, it's necessary to have the uXRCE-DDS client operating on PX4, connected with the micro XRCE-DDS agent running on the Jetson Nano. The PX4 uxrce_dds_client manages the publication and subscription of designated uORB topics within the global DDS data space. On the Jetson Nano, the eProsima micro XRCE-DDS agent serves as a proxy for the client within the DDS/ROS2 network.

Figure 3 presents the communication architecture based on ROS2 between the UAV modules (onboard computer, FCU, μC) and the ground station (computer and RC controller). The IMU, UWB, LiDAR, stereo camera and ESC nodes send (i.e. publish) and receive (i.e. subscribe) data via a number of topics while the buzzer and safety switch nodes send and receive data via services.

IV. RESULTS AND ANALYSIS

A. Weight Analysis

Given that the total takeoff weight (w_{TO}) of the electric multirotor UAV is represented as [19]

$$w_{TO} = w_0 + w_b + w_{pl} \tag{3}$$

where w_0 denotes the weight without the battery, consisting of the frame, avionics, and propulsion system, w_b indicates the battery weight, and w_pl represents the payload weight, including the onboard computer, camera, LiDAR, ultrasonic sensors and UWB tag. The UAV's total mass, excluding the battery, is a crucial factor in determining the battery size w_b.

Table I lists the breakdown of weights for the different components utilised in the quadcopter design. The take off weight of the quadcopter amounts to $\tilde{1}.5$ Kg with the Jetson Nano or 1.4 Kg with the Z-turn FPGA board.

B. Power Estimation

The power usage of a DC brushless motor may fluctuate based on several factors, including the motor's dimensions, operational voltage, and load circumstances. In essence, the power consumption of a DC brushless motor correlates directly with the mechanical power it delivers. Put simply, the greater the load the motor must propel, the more power it will consume.

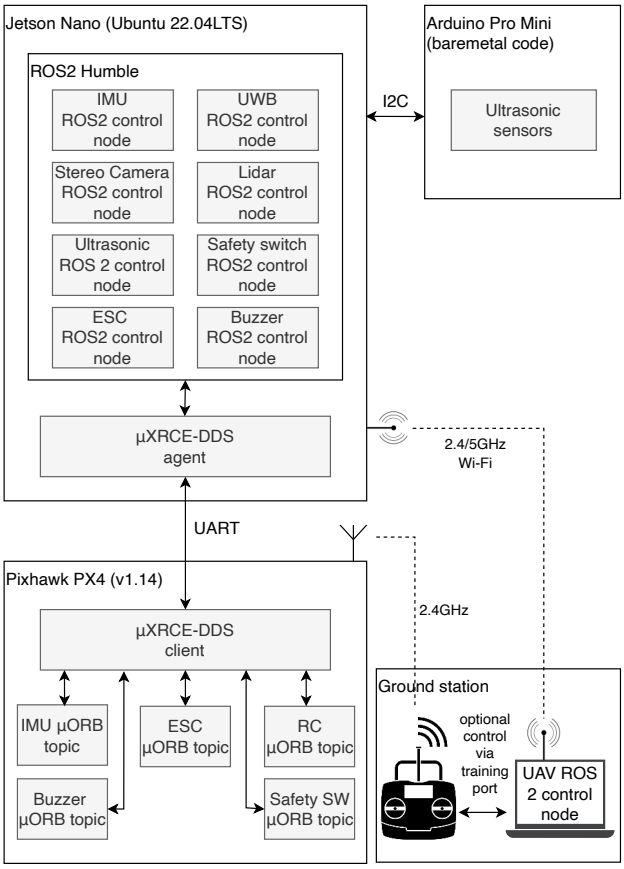

Fig. 3. ROS2 based communication architecture.

The power consumption (Watts) of a DC brushless motor can be determined using the formula

$$Power = Torque * Speed/9.55 \tag{4}$$

Here, torque (Nm) represents the force applied to the motor shaft, while speed denotes the motor's rotational speed in revolutions per minute (RPM)[4].

It's important to recognise that the power consumption of a DC brushless motor can also be influenced by the motor's efficiency, which may vary based on factors such as the motor's design and construction quality, the materials utilised, and the operating conditions.

LiPo batteries are popular choice for small UAVs given its high energy density and high current discharge capabilities [20]. As the battery constitutes a significant portion of the UAV's weight, choosing the appropriate one significantly affects flight duration. For the quadcopter platform, the aim is a flight duration of 10 to 15 minutes, with the battery discharged to 80% depth. Estimating the UAV's endurance, [21], involves calculating the battery energy and the power needed for hovering

$$E = \frac{E_b}{P_{h_e}} \tag{5}$$

[4]Speed in RPM is divided by $60/(2\pi)$ or 9.55 to convert it to radians per second (rad/s).

TABLE I

WEIGHT BREAKDOWN OF THE VARIOUS UAV PLATFORM COMPONENTS.

Quantity	Component Description	Weight (g)
1	F450 frame	270
4	Proppeler	56
4	Brushless DC Motor (1000KV)	208
4	Electronic speed controller	92
1	11.1V 4400mAh 3SP1 LiPo battery	340
1	Pixhawk P4 flight controller	16
1	NVIDIA Jetson Nano (MYiR Z-Turn)	142 (52)
2	DC-to-DC converter	10
1	RC receiver	6
4	Ultrasonic sensors	34
1	Arduino Pro Mini board	2
1	UWB Pozyx tag	42
1	ZED 2 stereo camera	160
1	Hokuyo UURG005	138
	Total weight	**1516 (1426)**

Here, E_b represents the battery energy, measured in watt-hours (Wh), while P_{h_e} is the electrical power necessary for the UAV to hover. Additionally, E_b can be expressed in relation to the battery's specific energy as

$$E_b = E_{spec} m_b n_b f_{DOD} \tag{6}$$

where E_{spec} represents the battery's specific energy, measured in Wh/kg, with typical values ranging between 50.7 and 220 Wh/kg for LiPo batteries [19]. In particular the E_{spec} can be defined as

$$E_{spec} = \frac{Cv}{m_b} \tag{7}$$

C represents the nominal battery capacity provided by the manufacturer, v is the nominal voltage between the leads, m_b denotes the mass of the battery, n_b indicates the battery efficiency, accounting for heat losses, and f_{DOD} represents the battery's depth of discharge (DOD) [19].

To prolong battery life, it is recommended not to discharge batteries beyond an 80% depth of discharge [22]. The power required for hover, P_{h_e}, is determined using momentum theory [23], calculated as follows (assuming an 80% motor efficiency as specified in the datasheet)

$$P_{h_e} = \left(\frac{W_{T_o}^{3/2}}{f\sqrt{2\rho\pi N_r} r_{prop}}\right)/0.8 \tag{8}$$

where, N_r represents the number of rotors with a radius of r_{prop}, ρ is the air density, and f denotes the figure of merit (propeller efficiency), which typically lies between between 0.5 and 0.7 [23]. In this work, a value of $f = 0.6$ is used.

From Eq.(5), (6) and (8), W_{TO} from Table I, $\rho = 1.225 kg/m^3$, $r_{prop} = 0.127m$ and $n_b = 95\%$ we get a preliminary estimated endurance of near 8 min. For a more accurate estimation of the UAV's endurance, the Peukert's model, as described in [22][24], could be employed, although this falls beyond the scope of the current study.

Table II illustrates the power consumption of the essential parts comprising the quadcopter. The Pozyx tag was intentionally not included in the table, as it is powered by a replaceable CR2450 (3 V, 620 mAh) battery, offering an

TABLE II

EXPECTED MAXIMUM POWER DRAW OF THE UAV COMPONENTS.

Component	Voltage (V)	Current (A)	Power (W)
BLDC (1000KV)	11.1	13	144.3
Pixhawk P4 (USB) inc. safety switch and buzzer	5	0.18	0.9
Jetson Nano	5	1-3	5-15
MYiR Z-Turn FPGA	5	1.6	8
RC receiver	5	0.03	1.5
Ultrasonic sensor	5	0.006	0.03
Arduino Pro Mini	5	0.016	0.08
LiDAR	5	0.5	2.5
ZED 2 stereo camera	5	0.38	1.9

autonomy of nearly 5 years according to the manufacturer's specifications. It's worth noting that powering the Pixhawk PX4 FCU via USB significantly reduces power consumption compared to powering it from the battery through the ESC, primarily due to the lower efficiency regulator in the ESC.

The complete multirotor UAV setup is shown in Fig.4.

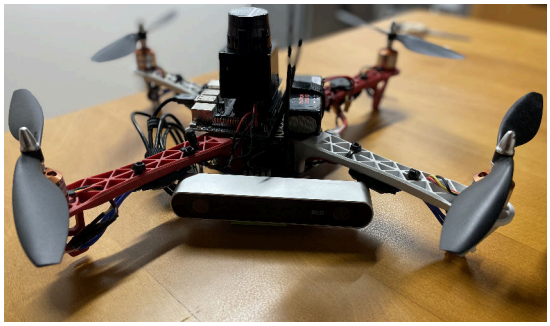

Fig. 4. Mutlirotor UAV implementation.

V. CONCLUSIONS AND FUTURE DIRECTIONS

We present a specialised hardware platform addressing the challenges of indoor navigation research with unmanned aerial vehicles (UAVs). While UAVs have become increasingly prevalent in research, particularly in aerial navigation, many proposed methodologies depend heavily on simulations, which may not accurately reflect real-world conditions. Our work introduces a low-cost modular UAV hardware platform specifically designed to enable research and development in aerial indoor navigation. By prioritising modularity, the platform offers researchers the flexibility to customise and scale their experiments to suit the unique requirements of indoor environments while meeting reasonable payload constraints. This approach not only speeds up the development process but also enables the evaluation of UAV navigation precision and reliability in real-world indoor scenarios.

The proposed UAV platform facilitates research and development, with the goal of conducting real-world experiments in complex indoor environments. The authors intend to utilise the UAV platform for performing real scenario experiments, building upon their prior research [4][5] that investigated the stability conditions of the classical Kalman filter (KF) and Maximum Correntropy Criterion Kalman filter (MCC-KF) algorithms in scenarios with packet drops.

REFERENCES

[1] S. A. H. Mohsan, N. Q. H. Othman, Y. Li, M. H. Alsharif, and M. A. Khan, "Unmanned aerial vehicles (uavs): Practical aspects, applications, open challenges, security issues, and future trends," *Intelligent Service Robotics*, vol. 16, no. 1, pp. 109–137, 2023.

[2] V. Pritzl, M. Vrba, P. Štěpán, and M. Saska, "Cooperative navigation and guidance of a micro-scale aerial vehicle by an accompanying uav using 3d lidar relative localization," in *2022 International Conference on Unmanned Aircraft Systems (ICUAS)*, 2022, pp. 526–535.

[3] J. Sandino, F. Vanegas, F. Maire, P. Caccetta, C. Sanderson, and F. Gonzalez, "Uav framework for autonomous onboard navigation and people/object detection in cluttered indoor environments," *Remote Sensing*, vol. 12, no. 20, p. 3386, 2020.

[4] L. Hadjiloizou, K. M. Deliparaschos, E. Makridis, and T. Charalambous, "Onboard Real-Time Multi-Sensor Pose Estimation for Indoor Quadrotor Navigation with Intermittent Communication," in *2022 IEEE Globecom Workshops (GC Wkshps)*, Dec. 2022, pp. 154–159.

[5] L. Hadjiloizou, E. Makridis, T. Charalambous, and K. M. Deliparaschos, "Maximum Correntropy Criterion Kalman Filter for Indoor Quadrotor Navigation under Intermittent Measurements," in *2023 31st Mediterranean Conference on Control and Automation (MED)*, June 2023, pp. 170–175.

[6] NVIDIA, "Jetson Nano Developer Kit," 2024. [Online]. Available: https://developer.nvidia.com/embedded/jetson-nano-developer-kit

[7] MYIR, "Z-turn Board," 2024. [Online]. Available: https://www.myirtech.com/list.asp?id=502

[8] C. Kallis, K. M. Deliparaschos, G. P. Moustris, A. Georgiou, and T. Charalambous, "Incremental 2D Delaunay triangulation core implementation on FPGA for surface reconstruction via high-level synthesis," in *2017 22nd IEEE International Conference on Emerging Technologies and Factory Automation (ETFA)*, Sept. 2017, pp. 1–4.

[9] Stereolabs, "ZED 2 - AI Stereo Camera," 2024. [Online]. Available: https://www.stereolabs.com/products/zed-2

[10] L. Zheng, P. Zhang, J. Tan, and F. Li, "The obstacle detection method of uav based on 2d lidar," *IEEE Access*, vol. PP, pp. 1–1, 11 2019.

[11] L. Kneip, F. Tache, G. Caprari, and R. Siegwart, "Characterization of the compact Hokuyo URG-04LX 2D laser range scanner," in *2009 IEEE International Conference on Robotics and Automation*, May 2009, pp. 1447–1454.

[12] J. Krejsa and S. Vechet, "The evaluation of hokuyo urg-04lx-ug01 laser range finder data," in *Eng. Mech. 2017*, Svratka, CZ, May 2017.

[13] Pozyx Labs, "Pozyx Labs - Accurate Positioning," 2024. [Online]. Available: https://www.pozyx.io

[14] F. Kendoul, D. Lara, I. Fantoni, and R. Lozano, "Nonlinear Control for Systems with Bounded Inputs: Real-Time Embedded Control Applied to UAVs," in *IEEE Conf. on Dec. and Con.*, 2006, pp. 5888–5893.

[15] H. Voos, "Nonlinear Control of a Quadrotor micro-UAV using Feedback-Linearization," in *IEEE International Conference on Mechatronics*, 2009, pp. 1–6.

[16] F. Sabatino, "Quadrotor Control: Modeling, Nonlinear Control Design, and Simulation," Master's thesis, KTH Royal Inst. of Tech., 2015.

[17] S. Bouabdallah, "Design and Control of Quadrotors with Application to Autonomous Flying," Ecole Polytechnique Fédérale de Lausanne (EPFL), Tech. Rep., 2007.

[18] eProsima, "eProsima Micro XRCE-DDS Agent," 2024. [Online]. Available: https://micro-xrce-dds.docs.eprosima.com/en/stable/agent.html

[19] M. Gatti, "Complete Preliminary Design Methodology for Electric Multirotor," *Journal of Aerospace Engineering*, vol. 30, May 2017.

[20] Y. N. Saravanakumar, M. T. H. Sultan, F. S. Shahar, W. Giernacki, A. Lukaszewicz, M. Nowakowski, A. Holovatyy, and S. Stepien, "Power Sources for Unmanned Aerial Vehicles: A State-of-the Art," *Applied Sciences*, vol. 13, no. 21, p. 11932, Jan. 2023.

[21] A. Kirenga, H.-I. Lee, and A. Zolotas, "Unmanned aerial system concept design for rail yard monitoring," in *AIAA SCITECH 2023 Forum*, 2023, p. 1733.

[22] M. Biczyski, R. Sehab, J. Whidborne, G. Krebs, and P. Luk, "Multirotor Sizing Methodology with Flight Time Estimation," *Journal of Advanced Transportation*, vol. 2020, pp. 1–14, Jan. 2020.

[23] L. Bauersfeld and D. Scaramuzza, "Range, Endurance, and Optimal Speed Estimates for Multicopters," *IEEE Robotics and Automation Letters*, vol. 7, no. 2, pp. 2953–2960, Apr. 2022.

[24] M.-h. Hwang, H.-R. Cha, and S. Y. Jung, "Practical endurance estimation for minimizing energy consumption of multirotor unmanned aerial vehicles," *Energies*, vol. 11, no. 9, p. 2221, 2018.

https://dspace.org/

A modular UAV hardware platform for aerial indoor navigation research and development

Deliparaschos, Kyriakos M.; Loizou, Savvas G.; Zolotas, Argyrios C.

2024-06-19
Institute of Electrical and Electronics Engineers (IEEE)
https://doi.org/10.1109/ICUAS60882.2024.10557007
Deliparaschos KM, Loizou SG, Zolotas AC. (2024) A modular UAV hardware platform for aerial indoor navigation research and development. In: IEEE 2024 International Conference on Unmanned Aircraft Systems (ICUAS) 4-7 June 2024, Chania - Crete, Greece. pp. 398-404

Downloaded from a DSpace repository. https://dspace.org/